

Determining the metric of the Cosmos: stability, accuracy, and consistency

M. L. McClure* and Charles Hellaby†
*Department of Mathematics & Applied Mathematics,
 University of Cape Town, Rondebosch 7701, South Africa*
 (Dated: March 28, 2008)

The ultimate application of Einstein’s field equations is to empirically determine the geometry of the Universe from its matter content, rather than simply assuming the Universe can be represented by a homogeneous model on all scales. Choosing an LTB model as the most convenient inhomogeneous model for the early stages of development, a data reduction procedure was recently validated using perfect test data. Here we simulate observational uncertainties and improve the previous numerical scheme to ensure that it will be usable with real data as soon as observational surveys are sufficiently deep and complete. Two regions require special treatment—the origin and the maximum in the areal radius. To minimize numerical errors near the origin, we use an LTB series expansion to provide the initial values for integrating the differential equations. We also use an improved method to match the numerical integration to the series expansion that bridges the region near the maximum in the areal radius. Because the mass enclosed within the maximum obeys a specific relationship, we show that it is possible to correct for a fixed systematic error in either the distance scale or the redshift-space mass density, such that the integrated values are consistent with the data at the maximum.

PACS numbers: 04.20.-q, 95.30.Sf, 98.65.Dx, 98.80.Jk

I. INTRODUCTION

Einstein’s equations relate the geometry of spacetime to the distribution of matter, and the most important application of this key physical concept is the study of the Universe. As the amount and precision of cosmological data improve, we will be able to determine not only the overall curvature of the Universe, but its detailed geometric structure too.

It is generally assumed that the Universe is homogeneous above the scale of superclusters and that it can be represented by a Friedmann-Lemaître-Robertson-Walker (FLRW) model. This assumption has served cosmology well and led to a very good understanding of many features of the observed Universe, which implies it cannot be seriously wrong. Yet it must be acknowledged that homogeneity is indeed an assumption that should eventually be checked against observations, once the data are sufficiently accurate and complete over a large enough range of redshifts. Because of our fixed position in the Universe, there are two distinct aspects to homogeneity—isotropy about our position, and uniformity with distance from us. Isotropy is relatively easy to check, but radial homogeneity has many intrinsic complications. Therefore a thorough verification will require considerable effort. The assumption of homogeneity is so pervasive, and underlies so much theoretical and observational work, that there is a real danger of a circular argument. Consequently, any proof of homogeneity must ensure it does not rely on results obtained using an assumption of homogeneity. Checking that the distribution of matter is homogeneous, while still using an FLRW model, is at best a consistency check and not a proof. A genuine proof must allow both the geometry and the matter to be inhomogeneous.

Historically, it has been theorized that it should be possible to use astronomical measurements to directly determine the metric of the Cosmos. The idea of co-ordinates based on the observer’s past null cone was first suggested by Temple [1], who called them “optical co-ordinates.” McCrea surveyed observational relations in homogeneous models [2] and was the first to determine them, as a series approximation, for inhomogeneous models [3]. Kristian and Sachs [4] were the first to consider the determination of a general metric for the Universe from observational data. They used series expansions near the observer in powers of diameter distance (and density field) for redshift, image distortion, number density, and proper motion. They considered the case of dust and estimated the parameters in their series, concluding that homogeneity was not proven. Ellis et al. [5] provided a major review of this problem. They showed it is not possible to obtain the spacetime metric without assuming Einstein’s field equations, and they also raised the problem of source evolution. Further papers by Stoeger, Nel, Maartens, Araujo, and others [6–14] considered

*Electronic address: mcclure@astro.utoronto.ca

†Electronic address: Charles.Hellaby@uct.ac.za

the fluid-ray tetrad, the spherically symmetric case and its perturbations, various solutions, and the origin conditions in these co-ordinates. Mustapha et al. [15] showed the diameter distance and the density observed on the past null cone can be significantly distorted by inhomogeneity. Ribeiro and Stoeger [16] considered the inclusion of a galaxy luminosity function, and checked catalogue data for consistency with the theory. A follow-up paper of Albani et al. [17] showed that analyses of galaxy statistics are strongly affected by the distance definition used.

Mustapha, Hellaby, and Ellis [18] considered data that are isotropic about us, and described an algorithm that could determine the specific Lemaître-Tolman-Bondi (LTB) model [19–21] that reproduces the observations. Thus, they claimed that any reasonable sets of observations of diameter or luminosity distance against redshift, and number counts against redshift, can be fit by an LTB model. They also showed that the effects of source evolution, cosmic evolution, and radial inhomogeneity are mixed together on the past null cone, and it is difficult to distinguish them. However, Hellaby [22] suggested a method of checking theories of source evolution in inhomogeneous geometries using multi-color observations. Célérier [23] considered a series expansion on the past null cone of an LTB model, and showed that the supernova data can be reproduced. Recently Célérier reviewed [24, 25] the need for inhomogeneous models in relation to observations, concluding that the standard methods of fitting a homogeneous universe to the data are open to significant systematic errors, and noting that fitting observations with inhomogeneous models is a significant challenge. Bishop and Haines [26] approached the Kristian and Sachs program as a time-reversed characteristic initial value problem, but they didn't solve the problem of the maximum in the diameter distance, and they only tested their numerical code with Einstein-de Sitter data.

Nevertheless, other than very limited series expansions, the various proposed methods have never been implemented with real data. Therefore we have begun a project to develop a numerical procedure that can do the necessary calculations and handle observational data. Thus, when sufficient data become available in the not-too-distant future, we will have a numerical routine capable of determining the Universe's spacetime structure.

The algorithm suggested by Mustapha, Hellaby, and Ellis [18] was implemented as a numerical procedure by Lu and Hellaby [27, 28]. The process of turning the algorithm into code raised some important issues that had not been obvious when discussing the theory. These include the fact that the real data are discrete, there are no data at the origin itself, and the differential equations to be solved are singular at the maximum in the areal radius, as well as the problem of the choice of appropriate numerical methods, given that the differential equations contain both observational data and the functions being solved for. The program was tested using ideal data, for a variety of homogeneous and inhomogeneous models, and successfully recovered the original models, thus demonstrating the viability of the method.

The main reason for working with spherical symmetry in these initial stages is merely to keep the theory and the numerics relatively simple. In the long run, this assumption will be dropped. However, there are three observational reasons why spherical symmetry is a good place to start. First, we note that we are at the center of our past null cone, so it makes sense to consider spacetime in terms of spherical co-ordinates. Second, the Universe does appear nearly isotropic on large scales, but radial homogeneity is not easy to verify because of the finite travel time of light and the miniscule duration over which cosmological observations have been made, so it is more urgent to determine the radial variation of the metric. Finally, there is no deep all-sky redshift survey at present, and the zone of avoidance is likely to be a gap in any survey for the foreseeable future.

If observations are made over the whole sky and the Universe is truly homogeneous on large scales, then using a spherically-symmetric model and binning the data over all angles should smear out any structures and lead to a radially-homogeneous metric at radii larger than the largest structures. At smaller radii the spherical shells may be enclosed entirely within a void or dominated by a supercluster and would appear inhomogeneous. Also, as a first check on isotropy, measurements made in different directions on the sky could be reduced separately, using our spherically-symmetric procedure, to look for angular variation.

The aim of the present paper is to extend the previous numerical routine of Lu and Hellaby [28] to be able to handle observational uncertainties. We study the stability of the differential equations used in the numerical routine, and how the uncertainties in the data should be propagated through the integration of the differential equations. We approximate the effect of random errors in observational data by adding Gaussian deviates to test data generated from model universes. Using this simulated data, we develop various improvements to the original numerical procedure, especially for calculating the derivatives of the areal radius, for dealing with the regions near the origin, and for matching the series expansion used about the maximum in the areal radius with the numerical integration regions on either side. Finally, we study the effect of systematic errors on the numerical algorithm and show that it is possible to correct for an overall systematic error in the distance scale or in the density (or if both are present, one may be corrected relative to the other to obtain a self-consistent result). Hellaby [29] showed that there is a relationship between the enclosed gravitational mass M , the areal radius R , and the cosmological constant Λ at the maximum in R that is independent of any inhomogeneity: this relationship is the key to detecting and correcting for systematic errors.

The main concern in this paper is the development of a basic numerical procedure that can handle input data

containing statistical and systematic errors. Of course, considerable processing is needed to extract the data functions needed by our numerical algorithm from the raw astronomical observations—luminosity functions, K-corrections, evolution of galaxies in luminosity and mass, galaxy mergers, etc.—and many sources of error must be considered in assessing the uncertainties. Though these must be carefully addressed in the future, for the present we assume that we are given data in the appropriate form with known uncertainties. It seems that type Ia supernovae are establishing themselves as very reliable standard candles out to redshifts well above 1, and when a sufficient number are measured, they may well provide the luminosity distance data for this project, or the basic calibration for a range of sources. Determination of the density of matter in redshift space, which is composed of the number density of sources and the mass per source, is much more problematic. The determination of masses from dynamics does extract the desired gravitational masses, but requires detailed observations, is not easy to do in large numbers, and can only be performed where there is luminous matter. It would be very convenient if there were a well-established tracer of mass that could be used instead of trying to count everything. There are some suggestions, such as luminous red galaxies, but it is very hard to demonstrate a certain type of source is a reliable tracer until a full mass census is taken over a region including several structures of all sizes. If the tracer sources are too widely dispersed, this would limit the scale on which inhomogeneity can be detected. Although current cosmological data are well short of the required quality and quantity, we expect dramatic improvements in accuracy and completeness in the not-too-distant future.

II. THE MODEL AND THE NULL CONE

We use the spherically-symmetric inhomogeneous-dust model (the “LTB” model) discovered by Lemaître, rediscovered by Tolman, and studied by Bondi [19–21]. We adhere to the notation used by Lu and Hellaby [28]. The metric is

$$ds^2 = -dt^2 + \frac{(R')^2}{1+2E} dr^2 + R^2 d\Omega^2, \quad (1)$$

where $d\Omega^2 = d\theta^2 + \sin^2\theta d\phi^2$, $R(t, r)$ is the areal radius, a prime denotes partial differentiation with respect to r , and the free function $E(r) \geq -1/2$ is a localized geometry term. From the Einstein field equations we get

$$\dot{R}^2 = \frac{2M(r)}{R} + 2E(r) + \frac{\Lambda R^2}{3}, \quad (2)$$

where $\dot{R} = \partial R / \partial t$, and

$$8\pi\rho = \frac{2M'}{R^2 R'}, \quad (3)$$

where $M(r)$ is a second free function that gives the gravitational mass within a comoving shell of radius r . Here $E(r)$ also plays the role of the local energy per unit mass of the dust particles. For the present we take $\Lambda = 0$, postponing more general considerations for later work. The solutions of (2), in terms of parameter η , are

$$E > 0: \quad R = \frac{M}{2E} (\cosh \eta - 1), \quad (\sinh \eta - \eta) = \frac{(2E)^{3/2}(t - t_B)}{M}; \quad (4)$$

$$E = 0: \quad R = M \left(\frac{\eta^2}{2} \right), \quad \left(\frac{\eta^3}{6} \right) = \frac{(t - t_B)}{M}; \quad (5)$$

$$E < 0: \quad R = \frac{M}{(-2E)} (1 - \cos \eta), \quad (\eta - \sin \eta) = \frac{(-2E)^{3/2}(t - t_B)}{M}; \quad (6)$$

for hyperbolic, parabolic, and elliptic evolution respectively. (Near the origin, where $E \rightarrow 0$, the type of evolution is determined by the sign of RE/M or $E/M^{2/3}$.) These solutions contain a third free function $t_B(r)$, which is the time of the big bang locally. By specifying the three free functions— $M(r)$, $E(r)$, and $t_B(r)$ —an LTB model is fully determined. Between them they provide a radial co-ordinate freedom and two physical relationships.

A. The observables and the differential equations

The background theory is presented in Section 2 of Lu and Hellaby [28], and here we merely summarize the essentials.

The diameter and luminosity¹ distances are

$$\hat{R} = d_D = \frac{D}{\delta}, \quad d_L = \sqrt{\frac{L}{\ell}} d_{10}, \quad (7)$$

where $D(z)$ and $L(z)$ are the true diameter and absolute luminosity of a source, δ and ℓ are the corresponding angular diameter and apparent luminosity, d_{10} is 10 parsecs, and they are related by the reciprocity theorem [30]²

$$(1+z)^2 d_D = d_L. \quad (8)$$

The redshift-space number density of sources n , measured in number per steradian per unit redshift interval, is related to the density ρ by ([18, 28])

$$\hat{R}^2 \hat{\rho} = \mu n \frac{dz}{dr}, \quad (9)$$

where μ is the mass per source.

Light rays arriving at the central observer follow $ds^2 = 0 = d\theta^2 = d\phi^2$, so the past null cone of the observation event $(t = t_0, r = 0)$ satisfies

$$\frac{dt}{dr} = -\frac{R'}{W}, \quad W = \sqrt{1 + 2E}, \quad (10)$$

and we write the solution $t = \hat{t}(r)$ or $r = \hat{r}(t)$. We denote a quantity evaluated on the observer's past null cone with a hat on top or as a subscript, for example $R(\hat{t}(r), r) \equiv \hat{R}$ or $[R]_{\wedge}$, though this will often be omitted where it is obvious from the context.

We can use the radial co-ordinate freedom to choose

$$\frac{d\hat{t}}{dr} = -1, \quad \text{i.e.} \quad \widehat{R'} = W, \quad (11)$$

on the observer's past null cone, so that the solution to (10) is

$$\hat{t} = t_0 - r. \quad (12)$$

Note that (11) and (12) and the following differential equations only hold for the single null cone with apex $(t_0, 0)$.

Since the co-ordinate r is not an observable, all r derivatives are converted to z derivatives, defining

$$\phi = \frac{dr}{dz} = -\frac{\frac{d\hat{R}}{dr}}{(1+z) \left(4\pi\mu n \frac{dz}{dr} + \frac{d^2\hat{R}}{dr^2} \right)} \quad (13)$$

and using

$$\frac{d\hat{R}}{dz} = \frac{d\hat{R}}{dr} \phi, \quad \frac{d^2\hat{R}}{dz^2} = \frac{d^2\hat{R}}{dr^2} \phi^2 + \frac{d\hat{R}}{dr} \frac{d\phi}{dz}. \quad (14)$$

Then from Lu and Hellaby [28], the differential equations are

$$\frac{dM}{dz} = 4\pi\mu n W, \quad (15)$$

$$W = \frac{1}{2\phi} \left(\frac{d\hat{R}}{dz} \right) + \frac{\left(1 - \frac{2M}{\hat{R}} \right) \phi}{2 \left(\frac{d\hat{R}}{dz} \right)} \quad (16)$$

¹ In Kristian and Sachs [4] a “corrected luminosity distance” was defined to be the same as the diameter distance. Some authors have called this the “luminosity distance,” which has led to a confusion of terminology and sometimes to incorrect definitions.

² This was first shown by Etherington [31]. Kristian and Sachs [4] cite a private communication from R. Penrose for a general proof of the reciprocity theorem, but we are not aware of any publication of that work.

and

$$\frac{d\phi}{dz} = \phi \left(\frac{1}{(1+z)} + \frac{\frac{4\pi\mu n\phi}{\hat{R}} + \frac{d^2\hat{R}}{dz^2}}{\frac{d\hat{R}}{dz}} \right). \quad (17)$$

Equations (13), (17), (15), and (16) constitute the differential equations (DEs) to be solved for $\phi(z)$, $r(z)$, $M(z)$, and $E(z)$. Then $t_B(z)$ follows from (4)-(6) and (12). Knowing $r(z)$, $M(z)$, $E(z)$, and $t_B(z)$ fully determines the LTB metric that reproduces the given $\hat{R}(z)$ and $\mu(z)n(z)$ data.

The LTB origin conditions were thoroughly examined in Mustapha and Hellaby [32], and Lu and Hellaby [28] give their application in this case.

B. Apparent horizon

The locus where the past null cone crosses the apparent horizon is also where the areal radius is maximum, i.e. the maximum \hat{R} is $\hat{R} = R_m$ at $z = z_m$. Since $d\hat{R}/dz = 0$ here, the DEs (17) and (15) with (16) become singular. However, it is obvious from (16) that where $d\hat{R}/dz = 0$ we must also have

$$\hat{R}_m = 2M_m, \quad (18)$$

since W is arbitrary (see Krasiński and Hellaby [33], Hellaby [34]). Similarly (13) and (17) show that

$$\left. \frac{d^2\hat{R}}{dr^2} \right|_m \phi_m = -4\pi\mu_m n_m, \quad \left. \frac{d^2\hat{R}}{dz^2} \right|_m = -4\pi\mu_m n_m \phi_m, \quad (19)$$

since we don't expect dz/dr or d^2r/dz^2 to be divergent here in a general LTB model with co-ordinate choice (11). Indeed, (18) and (19) are exactly what happens at \hat{R}_m in the FLRW case. So although there are no divergencies at \hat{R}_m , the numerics break down. In Lu and Hellaby [28] this was overcome by doing a series expansion in $\Delta z = z - z_m$, and joining the numerical and series results at some z value $z_a < z_m$ —see sections 2.6, 3.3, and appendix B of their paper. As pointed out by Hellaby [29], this phenomenon is not merely a cosmological curiosity. At this locus, and no other, there is a simple relation between the diameter distance $d_D = \hat{R}$ and the gravitational mass M_m that is independent of any inhomogeneity between the observer and sources at this distance:

$$2M_m = \hat{R}_m - \frac{\Lambda \hat{R}_m^3}{3}, \quad (20)$$

or (18) if $\Lambda = 0$. (However, the redshift z_m at which this occurs is model dependent.) Therefore the maximum in \hat{R} provides a new characterization of our Cosmos—the cosmic mass. More importantly for this paper, it provides a cross-check on the numerical integration, since the M value obtained from the numerical integration must agree with that deduced from the measured \hat{R}_m using (18) or (20). For this reason, it plays a prominent role in what follows.

C. Outline of numerical procedure

Since the long-term intent is to use observational data as input, some important practical considerations arise, as discussed in Lu and Hellaby [28]. The above analysis assumes continuous functions and differential equations, whereas real cosmological data consist of a large number of discrete measurements of individual sources (e.g. galaxies); and numerical integration involves discrete steps of finite size.

Measurements of the magnitudes (or luminosities) and masses of individual galaxies involve considerable uncertainty, so it is advisable to average over a significant sample, and this requires putting the data into redshift bins. (At present, bins of width $\delta z = 0.001$ are being used.) While redshift measurements are relatively accurate, the observed redshifts include peculiar velocities, so again bin averages reduce the uncertainty³. The very-low z bins⁴ are strongly affected

³ Actually, the diameter distance is unaffected by peculiar velocity, even if it is calculated from the luminosity distance and the redshift using the reciprocity formula (8). Therefore, if measurements of diameter distance or luminosity distance become sufficiently accurate out to large redshifts, it would be preferable to bin the data by $d_D = \hat{R}$. The main difficulty would be to distinguish sources just closer and just farther than the maximum in \hat{R} .

⁴ If we could detect all sources, the low- z bins would have very little data, but in fact the data are far more complete at low z , so the

by peculiar velocities, and there are no data at the origin itself, which makes it difficult to set the initial conditions for the DEs. Thus, we have to estimate the origin values from the data in the low- z data bins and a series expansion of the model. Therefore the procedure for integrating down the PNC has four main stages: the origin fitting, the first numerical integration interval, the near maximum series, and the second numerical integration.

Because the DEs involve the first and second derivatives of the observational quantity $\hat{R}(z)$, it is evident that noise in this function could create very large fluctuations in the derivatives. Thus, in addition to binning the data, it may be necessary to smooth out statistical fluctuations by fitting a curve to the binned data.

Each of the procedures—binning, smoothing, numerical integration procedure, etc.—is a potential source of unintended bias and obviously determines the smallest scale on which inhomogeneity can be detected. So it is likely that our thinking about the best way to handle all these issues will evolve as the project proceeds.

The next two sections consider the effect of statistical uncertainty in the data functions $\hat{R}(z)$ and $4\pi\mu n(z)$. This affects both the uncertainty in the output functions $M(z)$, $E(z)$ and $t_B(z)$, and the stability of the solution procedure.

III. STABILITY OF THE DIFFERENTIAL EQUATIONS

A. Equations for r and ϕ

The co-ordinate distance r is calculated by integrating (13), once $\phi = dr/dz$ has been determined from (17),

$$\frac{d\phi}{dz} = \phi_z = \left(\frac{1}{1+z} + \frac{\hat{R}_{zz}}{\hat{R}_z} + \frac{4\pi\mu n\phi}{\hat{R}\hat{R}_z} \right) \phi, \quad (21)$$

where z subscripts denote differentiation with respect to z . The expression for the error in ϕ_z due to the error in ϕ is

$$\Delta\phi_z = \left(\frac{\phi_z}{\phi} + \frac{4\pi\mu n\phi}{\hat{R}\hat{R}_z} \right) \Delta\phi, \quad (22)$$

which holds only for $\Delta\phi \ll \phi$. At small z , the $4\pi\mu n\phi/(\hat{R}\hat{R}_z)$ term is insignificant relative to the other two terms in ϕ_z at $z = 0$, and $\hat{R}_z > 0$ before the maximum in \hat{R} , so this leads to the integrated values of ϕ being stable so long as ϕ_z is negative and ϕ is positive. When ϕ_z is stable, if ϕ is over (or under) estimated, then the factor of ϕ in ϕ_z leads to ϕ_z being under (or over) estimated so that ϕ opposingly decreases (or increases) toward the correct value. It is possible for ϕ to become unstable if ϕ_z becomes positive; however, this should only occur if there are strong inhomogeneities, and only over a small range of z , meaning the instability can only grow over a short range before ϕ becomes stable again and corrects itself.

Beyond the overall influence of the ϕ factor in ϕ_z , there is an additional ϕ in the third term of ϕ_z that can lead to instability before the maximum in \hat{R} . As the maximum \hat{R}_m is approached, the $4\pi\mu n\phi/\hat{R}\hat{R}_z$ term grows faster than ϕ_z/ϕ , and after the point where

$$\frac{\hat{R}_{zz}}{\hat{R}_z} = - \left(\frac{1}{1+z} + \frac{8\pi\mu n\phi}{\hat{R}\hat{R}_z} \right) \quad (23)$$

the DE becomes increasingly unstable towards \hat{R}_m . Near the maximum, the terms in (21) involving $1/\hat{R}_z$ both diverge, but they ought to cancel with ideal data and calculations, because $\hat{R}_{zz} = 4\pi\mu n\phi/\hat{R}$ at \hat{R}_m . Since the sign of \hat{R}_z must change from positive to negative at \hat{R}_m , while all other quantities maintain the same sign, then ϕ returns to being stable after \hat{R}_m .

Since the values of r are integrated using the values of ϕ , the stability in r depends on the stability in ϕ . The main difference is that if ϕ diverges in one direction and later stabilizes back to the proper value, there is a cumulative impact on the integrated values of r , so the consequence of any instability in ϕ is potentially worse for r . The integration relies on the use of a series expansion to get past the maximum in \hat{R} . Provided the integration switches over to the series expansion well enough in advance of the maximum, then ϕ should not diverge significantly from the correct value, and the cumulative effect on r should not be significant.

opposite is true.

B. Equations for M and E

The differential equation (15) with (16) for M is given by

$$\frac{dM}{dz} = M_z = 4\pi\mu nW, \quad (24)$$

where

$$W = \sqrt{1 + 2E} = \frac{\hat{R}_z}{2\phi} + \left(1 - \frac{2M}{\hat{R}}\right) \frac{\phi}{2\hat{R}_z}, \quad (25)$$

and so the stability equation for $\Delta M \ll M$ is

$$\Delta M_z = 4\pi\mu n \left[\left\{ -\frac{\hat{R}_z}{2\phi^2} + \left(1 - \frac{2M}{\hat{R}}\right) \frac{1}{2\hat{R}_z} \right\} \Delta\phi - \frac{\phi}{\hat{R}\hat{R}_z} \Delta M \right]. \quad (26)$$

Since W contains a term that goes as $-M\phi/(\hat{R}\hat{R}_z)$, if M is over (or under) estimated, then W , E , M_z , and M are opposingly under (or over) estimated when \hat{R}_z is positive, making the determination of M from W stable and the determination of W (and E) from M stable. Barring the presence of strong inhomogeneities, \hat{R}_z should remain positive out to the maximum in \hat{R} , so M and W should remain stable with each other up to the maximum. If there are strong inhomogeneities, these should only make \hat{R}_z go negative over short regions of the integration, meaning the instability can only grow briefly before M and W become stable and return to their proper values. The values of W , E , M_z , and M also depend on the integrated values of ϕ , so if ϕ becomes unstable, as it may do before the maximum, then W and M can potentially become unstable due to ϕ , but as discussed previously, the series expansion of ϕ around the maximum should bridge this instability in ϕ .

After the maximum in \hat{R} , \hat{R}_z should remain negative (except in the presence of strong inhomogeneities), which means over (or under) estimates in M lead to over (or under) estimates in W and E , and over (or under) estimates in W lead to over (or under) estimates in M_z and M . Thus, M and W feed back on each other and lead to instability. This suggests an alternative method is needed to determine M and E after the maximum in \hat{R} is reached. Assuming the data do not extend significantly beyond the maximum, one method is to create an extended series expansion in W based on the $4\pi\mu n$ and \hat{R} data from the maximum to the outer boundary, and then integrate values of M based on the W series expansion so that M and W do not feed back on each other. If the data extend significantly beyond the maximum, and no alternative method is found, we must expect very large uncertainties in W and M .

IV. NUMERICAL HANDLING OF STATISTICAL ERRORS

A. Simulating errors with Gaussian deviates

In order to make sure the code can handle real data, statistical errors must be added to the distance determinations and galaxy number counts for the test data.

The actual number of sources N per bin is equal to $4\pi n\delta z$ (where δz is the redshift interval of the bin), since n is the number of sources per steradian and per unit redshift interval. From the test universes, the number of sources N is calculated as

$$N = \frac{4\pi\mu n\delta z}{\mu}, \quad (27)$$

where μ is the assumed mass of a typical galaxy— $10^{11} M_\odot$. The program then calculates the expected errors in the \hat{R} and $4\pi\mu n$ values by calculating the $1\text{-}\sigma$ errors and using the elimination method to add Gaussian deviates (e.g. [35]) to the data in a $\pm 5\sigma$ range.

The random error in a single \hat{R} measurement is assumed to be of order 10% so that the random error $\Delta\hat{R}$ in the \hat{R} value for a bin of N galaxy sources is

$$\Delta\hat{R} = \frac{0.1\hat{R}}{\sqrt{N}}. \quad (28)$$

(Although current luminosity-distance measurements are mostly not this good, it is expected the accuracy will improve considerably in the coming years.)

The random error in the $4\pi\mu n$ measurements is

$$\Delta(4\pi\mu n) = \frac{1}{\delta z} \sqrt{(\Delta\mu N)^2 + (\Delta N \mu)^2} = \frac{1}{\delta z} \sqrt{(\Delta m \Delta N)^2 + (\Delta N \mu)^2}, \quad (29)$$

where $\Delta N = \sqrt{N}$, and $\Delta\mu = \Delta m / \Delta N$ relates the error in the mean mass per source μ and the error in a single mass measurement m . The uncertainty in N is calculated using the Poisson error, since if the galaxies occur randomly, then the uncertainty in the number that should be observed goes as \sqrt{N} . (In reality galaxies are clustered, but since we are binning over thin spherical shells, clusters will be averaged out at large radii.) Assuming Δm is less than (or of the same order as) μ , then the random error in the $4\pi\mu n$ measurements is approximately

$$\Delta(4\pi\mu n) = \frac{\mu\sqrt{N}}{\delta z} = \frac{4\pi\mu n}{\sqrt{N}}. \quad (30)$$

B. Calculating derivatives of \hat{R}

With errors in the \hat{R} values, it is no longer possible to use the original method of Lu and Hellaby [28] of calculating the first and second derivatives, which were obtained from the first and second differences in \hat{R} between adjacent redshift bins. Due to errors in the data, the noise in the second derivative ends up being of order 10000%. This causes the integrated values of ϕ to vary rapidly up and down and quickly diverge shortly after the instability in ϕ develops (before the maximum in \hat{R}).

Thus, in order to reduce the noise in the derivatives, it is necessary to calculate least-squares fits to the \hat{R} data. Unfortunately, since the functional form of $\hat{R}(z)$ cannot be assumed, simply fitting a single polynomial is unlikely to yield a good fit over the whole range of data. Rather, the values of the first and second derivatives that best reflect the local data are obtained by fitting a polynomial to the $2k+1$ redshift bins centered on each z_i , covering the range $z_i \pm k\delta z$. Since variations in the second derivative should exist, especially if strong inhomogeneities are present, it is necessary to use at least a cubic polynomial, so that the second derivative is allowed to vary over the range of the fit. Near the origin and outer boundary, it is not possible to have a range of data that is centered exactly on the point in interest, making it even more important to have at least a quartic fit so that the unequal upper and lower ranges of data do not bias the calculation of the second derivative.

When there are strong variations in \hat{R}_{zz} , it is necessary to either reduce the range of data used in the fit or increase the order of the fit so that they do not get smoothed out. In either case this leads to more noise in the fit. The ideal data range and polynomial order varies depending on the test universe. If there are no strong variations it is better to use a lower order polynomial (such as a quartic) and a large range of data (up to 300 redshift bins centered on the current z value) to reduce the noise, but when there are strong variations, it is better to increase the order or reduce the range to allow some noise, in the interest of fitting the actual variation. It is obvious if real variations are present, since these are noticeable even in the lower-order fits where the noise is negligible. Exactly how much the range should be reduced or the order of the polynomial should be increased can be ascertained by changing the fit until the real variations cease to become stronger or when the noise starts to become a significant fraction of the magnitude of the real variation. In practice, for the test model with strongest inhomogeneity, the range could be as small as 30 δz bins and the fit as high as 7th order.

More precisely, the best polynomial fit to the data can be ascertained by comparing the ratio of χ^2 with the number of degrees of freedom (NDF), where χ^2 is the sum of the squares of the \hat{R} residuals divided by the 1- σ error of each \hat{R} value, and the NDF is the number of data points minus the number of polynomial coefficients being fit. The expected value of χ^2 is the NDF, so the ratio of the two that is closest to 1 yields the best fit to the data. A ratio greater than 1 is not adequately fitting the data, while a ratio smaller than 1 is fitting the data too well, which means it is likely fitting the noise and is not the most realistic fit to the data.

It should be noted that the least-squares fitting of \hat{R} versus z minimizes the error in the \hat{R} values, so it assumes no error in z . Any actual errors in z would bias the fit. While the observational errors in z should be small, the peculiar velocity components of the observed redshifts may lead to errors.

Another consequence of this smoothing is that random fluctuations in the \hat{R} data create quasi-periodic variations in the smoothed versions of \hat{R} , \hat{R}_z , and \hat{R}_{zz} , which have a period determined by the z range chosen for the fit. These manifest themselves in ϕ as oscillations with an amplitude that diverges as the maximum \hat{R}_m is approached.

C. Using an origin LTB series expansion

The integration of the differential equations must proceed from an initial value, which in the original code of Lu and Hellaby [28] involved using an FLRW series expansion at the origin to determine the derivatives in the first two redshift bins. Since a regular LTB model is FLRW-like at the origin, this is not a bad first approximation. However, the fractional errors in \hat{R} and $4\pi\mu n$ are largest near the origin, due to the smaller number counts that occur in a bin of given thickness δz , and also, the \hat{R} derivatives are more susceptible to error near the origin. The determination of the bang time is more difficult near the origin, because this depends on $2E\hat{R}/M$, while E , R , and M are all approaching zero and highly susceptible to numerical errors. Thus, it is preferable to use the series expansion for more than just the first two bins, which necessitates the use of an LTB series so that the region around the origin is not constrained to be FLRW. Approximating \hat{R} and $4\pi\mu n$ near the origin by 5th order power series in z , the series coefficients are found by a least-squares fit to the data in the first 50 bins (which extends to $z = 0.05$ —a distance scale at which there should be adequate data to begin integrating from bin to bin without large numerical errors). The functions ϕ , M , and E are also expressed as power series, and their coefficients are derived from the DEs. The values of the functions at the end of the origin series then provide the initial conditions for the numerical integration.

Series expansions of the \hat{R} and $4\pi\mu n$ data near the origin in the form

$$\hat{R}(z) = R_1 z + R_2 z^2 + R_3 z^3 + R_4 z^4 + R_5 z^5 \quad (31)$$

and

$$4\pi\mu n(z) = K_2 z^2 + K_3 z^3 + K_4 z^4 + K_5 z^5 \quad (32)$$

are used to calculate the series expansions of r , ϕ , M , and $2E$ from (17), (13), (15), and (16), as

$$\begin{aligned} r(z) = & R_1 z + \left(\frac{R_1}{2} + R_2\right) z^2 + \left(\frac{2R_2}{3} + R_3 + \frac{K_2}{6}\right) z^3 + \left(\frac{3R_3}{4} + \frac{5K_2}{24} + R_4 + \frac{K_3}{12} + \frac{K_2 R_2}{6R_1}\right) z^4 \\ & + \left(R_5 + \frac{K_4}{20} + \frac{7K_3}{60} + \frac{K_2}{15} + \frac{4R_4}{5} + \frac{\left(\frac{K_3}{12} + \frac{13K_2}{60}\right)R_2 + \frac{K_2 R_3}{4} + \frac{K_2^2}{20}}{R_1} - \frac{K_2 R_2^2}{12R_1^2}\right) z^5, \end{aligned} \quad (33)$$

$$\begin{aligned} \phi(z) = & R_1 + 2\left(\frac{R_1}{2} + R_2\right) z + 3\left(\frac{2R_2}{3} + R_3 + \frac{K_2}{6}\right) z^2 + 4\left(\frac{3R_3}{4} + \frac{5K_2}{24} + R_4 + \frac{K_3}{12} + \frac{K_2 R_2}{6R_1}\right) z^3 \\ & + 5\left(R_5 + \frac{K_4}{20} + \frac{7K_3}{60} + \frac{K_2}{15} + \frac{4R_4}{5} + \frac{\left(\frac{K_3}{12} + \frac{13K_2}{60}\right)R_2 + \frac{K_2 R_3}{4} + \frac{K_2^2}{20}}{R_1} - \frac{K_2 R_2^2}{12R_1^2}\right) z^4, \end{aligned} \quad (34)$$

$$\begin{aligned} M(z) = & \frac{K_2}{3} z^3 + \frac{K_3}{4} z^4 + \left(\frac{-K_2^2}{15R_1} + \frac{K_2}{10} + \frac{K_4}{5}\right) z^5 \\ & + \left(\left(\frac{1}{36R_1} + \frac{R_2}{18R_1^2}\right) K_2^2 + \left(\frac{-1}{12} - \frac{7K_3}{72R_1}\right) K_2 + \frac{K_3}{12} + \frac{K_5}{6}\right) z^6, \end{aligned} \quad (35)$$

and

$$\begin{aligned} E(z) = & \left(\frac{1}{2} - \frac{K_2}{3R_1}\right) z^2 + \left(\left(\frac{1}{6R_1} + \frac{R_2}{3R_1^2}\right) K_2 - \frac{1}{2} - \frac{K_3}{4R_1}\right) z^3 \\ & + \left(\frac{29K_2^2}{360R_1^2} + \left(-\frac{11}{60R_1} + \frac{R_3}{3R_1^2} - \frac{R_2^2}{3R_1^3}\right) K_2 + \left(\frac{1}{12R_1} + \frac{R_2}{4R_1^2}\right) K_3 + \frac{5}{8} - \frac{K_4}{5R_1}\right) z^4 \\ & + \left(\left(-\frac{1}{360R_1^2} - \frac{11R_2}{90R_1^3}\right) K_2^2 + \left(\frac{K_3}{9R_1^2} + \frac{19}{60R_1} + \frac{\frac{11R_2}{60} + \frac{R_4}{3} + \frac{R_3}{12}}{R_1^2} + \frac{-\frac{2R_2 R_3}{3} - \frac{R_2^2}{12}}{R_1^3} + \frac{R_2^3}{3R_1^4}\right) K_2 \right. \\ & \left. + \left(-\frac{1}{8R_1} + \frac{R_3}{4R_1^2} - \frac{R_2^2}{4R_1^3}\right) K_3 + \left(\frac{1}{20R_1} + \frac{R_2}{5R_1^2}\right) K_4 - \frac{3}{4} - \frac{K_5}{6R_1}\right) z^5. \end{aligned} \quad (36)$$

In Figure 1, the relative error in the bang time near the origin is shown for both the previous method and the new method. The large numerical error that occurs with the previous method is greatly reduced by using the LTB series expansion.

D. Bridging the maximum in the areal distance

Since, as noted in Section IIB, \hat{R}_z goes to zero at \hat{R}_m (the maximum in \hat{R}), and the DEs for ϕ (17) and M (15) and (16) both depend on $1/\hat{R}_z$, it is necessary to use a series expansion in the neighborhood of the maximum. Also,

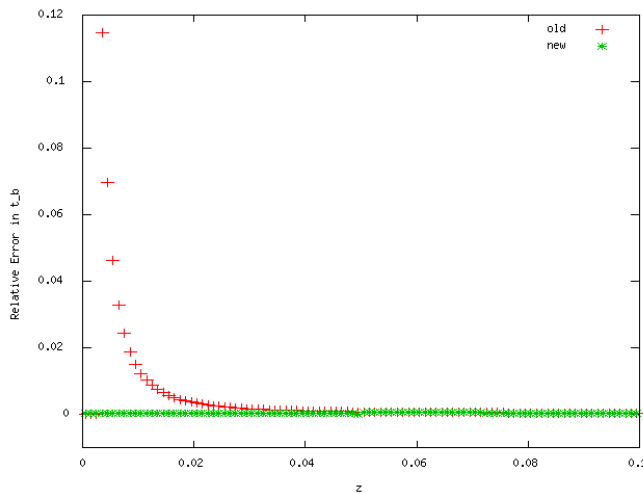


FIG. 1: Comparison of the relative errors in the bang time t_B versus z using the old (crosses) and new (asterisks) methods. The new method fits an LTB series expansion to the first 50 points, before starting the numerical integration, thus allowing the solution to be inhomogeneous while avoiding the numerical difficulties near the origin. This plot is for an inhomogeneous universe with origin Hubble and deceleration parameters $h_0 = 0.72$ and $q_0 = 0.6$, and with $\Omega_\Lambda = 0$.

the ϕ DE becomes unstable before the maximum, so this series expansion is necessary over a range of more than just a few points.

Appendix A gives the series solutions for ϕ , M , and W in powers of $\Delta z = z_m - z$. The coefficients in the ϕ series are fully determined by the DEs, but the M and W coefficients are interrelated and contain one undetermined coefficient, the linear term in the M series, or equivalently, the constant term in the W series. In fact every coefficient of the M and W series depends linearly on this factor, so its value is easily fixed by matching these two series to their numerical values at some cross-over point $z = z_a < z_m$, where the series and numerical ϕ curves are in closest agreement, as was done by Lu and Hellaby [28]. A second matching is done at $z = z_J > z_m$, where the near-maximum series ends and the numerical integration is re-started.

When statistical errors are present however, the oscillations in ϕ that grow as \hat{R}_m is approached make the matching of the numerical and series ϕ values problematic, since they will tend to intersect at multiple points. Thus, the code has been modified such that the two ϕ curves are matched by calculating the absolute value of the differences between the curves over a range of the data (the same range used in the least-squares fit of \hat{R}) and matching them at the z value where the total difference is minimized. This generally leads to a matching near where the ϕ instability sets in, thus excising the region of diverging ϕ error.

In the original code of Lu and Hellaby [28], M was matched at the start of the series, and W was matched at the end of the series. While M and W are stable with each other before \hat{R}_m , the fluctuations in ϕ influence W , which oppositely influences M , so typically there is a small error in M at the first matching point. This M matching error biases the slope of the M series, and in turn the constant term of the W series. Thus, there is generally a small jump in W at the first matching point and a small jump in M at the second matching point, which in turn leads to a rapid adjustment in W once the numerical integration re-starts.

However, it turns out that it is possible to find values of M and W that are consistent with each other at the first matching point so that the small error in M does not lead to overcorrections. The mean of the integrated value of M and the value of M that would result from matching the integrated value of W is used to determine the series-connection value of M . Similarly, the mean of the integrated value of W and the value of W that would result from matching the integrated value of M determines the series-connection value of W . These new series-connection values of M and W are consistent with each other in that calculating the M -series matching using the mean W value for the matching leads exactly to the mean M value, and vice versa for the mean W value. Also, these values are stable in that calculating the matching with “numerical” values above (or below) the mean results in series-connection values closer to the mean values. This can be explained by the fact that M and W are stable with each other before \hat{R}_m , so there should be stable series expansion values of M and W that are consistent with each other before \hat{R}_m .

Plots of the relative error in M and W in the region containing the matching before \hat{R}_m appear in Figure 2. Using this new matching method reduces the jump in W at the first matching so that it does not overcorrect, and it leads to more accurate values of W throughout the series expansion. It also leads to more accurate values of M in the

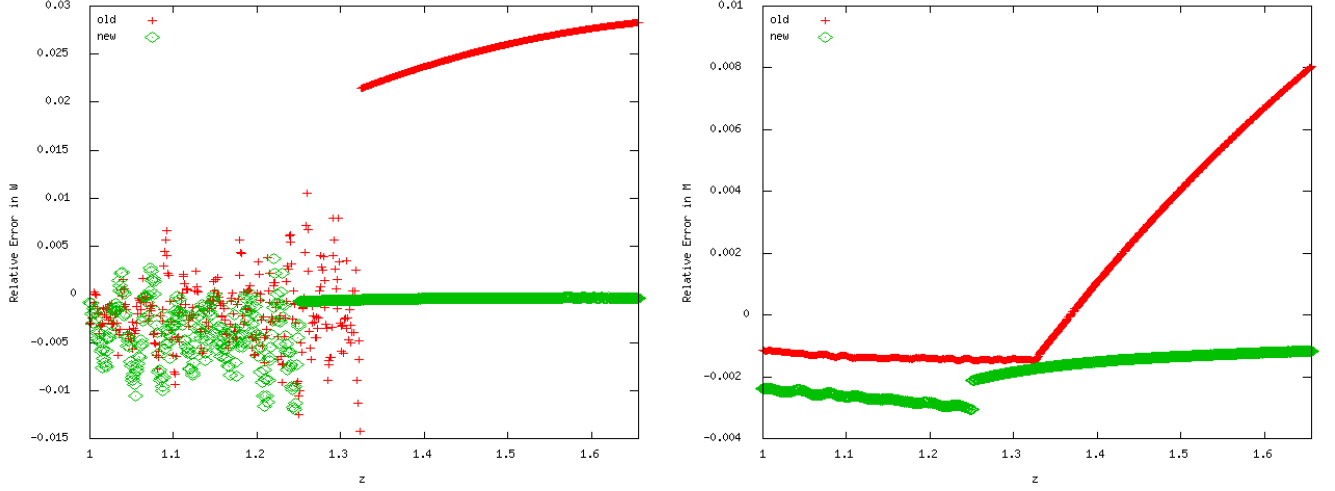


FIG. 2: Comparison of the relative errors in W (left) and M (right) versus z in the region before \hat{R}_m , using the old (small crosses) and new (large diamonds) methods for matching from the numerical values to the near-maximum series expansion values. These plots are for an FLRW universe with $h_0 = 0.72$, $q_0 = 0.22$, and $\Omega_\Lambda = 0$, with statistical errors added to the data to simulate observational errors. Simply matching M can lead to a large jump in W and a divergence in M , whereas the new method leads to small jumps in both M and W that always bring them toward the correct values.

near-maximum series, and much better values of M at the second matching. This is an important improvement over the original code, especially when there are errors in the data that can lead to larger jumps in M and W .

E. Propagation of uncertainties

To estimate the uncertainties, the observational errors need to be taken into account in how they propagate in the integrations. Where a series fit to the data is performed, the estimated errors come from the covariance matrix of the fit. The uncertainties in the numerical integration of r_z , ϕ_z , W , and M_z are

$$\Delta r_z = \Delta \phi, \quad (37)$$

$$\begin{aligned} \Delta \phi_z = & \left(\left[\left(\frac{1}{1+z} + \frac{\hat{R}_{zz}}{\hat{R}_z} + \frac{8\pi\mu n\phi}{\hat{R}\hat{R}_z} \right) \Delta \phi \right]^2 + \left(\frac{\phi}{\hat{R}_z} \Delta \hat{R}_{zz} \right)^2 + \left[\left(\frac{\hat{R}_{zz}\phi}{\hat{R}_z^2} + \frac{4\pi\mu n\phi^2}{\hat{R}\hat{R}_z^2} \right) \Delta \hat{R}_z \right]^2 \right. \\ & \left. + \left(\frac{4\pi\mu n\phi^2}{\hat{R}^2\hat{R}_z} \Delta \hat{R} \right)^2 + \left(\frac{\phi^2}{\hat{R}\hat{R}_z} \Delta(4\pi\mu n) \right)^2 + \left(\frac{1}{(1+z)^2} \Delta z \right)^2 \right)^{1/2}, \end{aligned} \quad (38)$$

$$\Delta W = \left(\left[\left(\frac{\hat{R}_z}{2\phi^2} - \frac{1-2M/\hat{R}}{2\hat{R}_z} \right) \Delta \phi \right]^2 + \left[\left(\frac{1}{2\phi} - \frac{(1-2M/\hat{R})\phi}{2\hat{R}_z^2} \right) \Delta \hat{R}_z \right]^2 + \left(\frac{M\phi}{\hat{R}\hat{R}_z^2} \Delta \hat{R} \right)^2 + \left(\frac{\phi}{\hat{R}\hat{R}_z} \Delta M \right)^2 \right)^{1/2}, \quad (39)$$

and

$$\Delta M_z = \left(\left[(W\Delta(4\pi\mu n))^2 + (4\pi\mu n\Delta W)^2 \right] \right)^{1/2}, \quad (40)$$

assuming that the errors are uncorrelated with each other so that they are added in quadrature.

The ϕ_z values are used to calculate each ϕ value from the previous ϕ value, but how the error in ϕ accumulates depends on the stability in ϕ . It would be expected that when ϕ is stable this error would not grow from step to step, while when ϕ is unstable the errors from all the unstable steps would need to be added together directly. In practice, calculating the ϕ uncertainty is more complicated, due to the smoothing of the \hat{R} data. The errors in the smoothed \hat{R}_{zz} values tend to fluctuate up and down with a period $\zeta = 2k\delta z$ equal to the range of data that is used to perform the least-squares fit. These fluctuations in the \hat{R}_{zz} errors induce fluctuations in the ϕ values, so even when ϕ is stable it tends to oscillate with the same period as the range of the least-squares fit. However, over a range $\geq \zeta$, the errors due to the fluctuations tend to cancel, and so should not be added continuously.

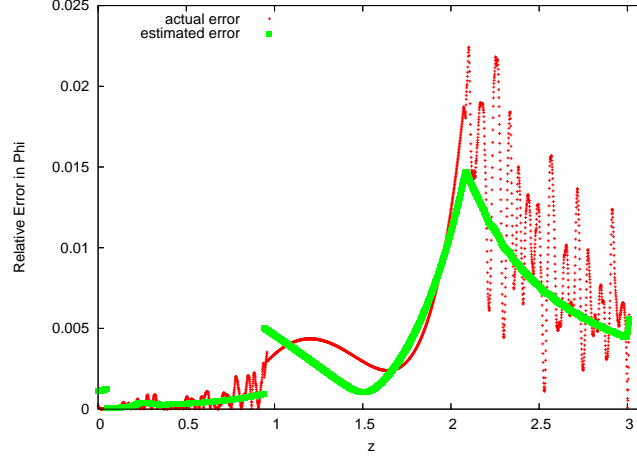


FIG. 3: Relative ϕ error versus z , with the estimated error (large points) plotted alongside the actual error (small points) for comparison. Gaussian deviates are added to the data, and the estimated uncertainty calculated, along with the actual error from the ideal data. It can be seen that the error in ϕ grows before the maximum as it becomes increasingly unstable, and then decreases after the maximum as it becomes stable again. This plot is for an inhomogeneous universe with origin parameters $h_0 = 0.72$, $q_0 = 0.6$, and $\Omega_\Lambda = 0$.

The actual calculation of the ϕ uncertainty proceeds by taking the errors of all the previous steps that may potentially be continuously fluctuating in one direction (starting either from the initial point of integration or at a point that is previous to the point of interest z_i by half the range of the \hat{R} fit, $\zeta/2$) and adding these in quadrature (since the errors at these steps are unlikely to all be of the same sign) to get the error due to the fluctuations $\Delta\phi_f$:

$$\Delta\phi_f = \sum_{j=i-\zeta}^i \Delta\phi_z[j] \delta z, \quad (41)$$

and combining this error with the error $\Delta\phi_s$ from the end of the series leading up to the numerical integration by adding them in quadrature:

$$\Delta\phi = \sqrt{(\Delta\phi_s)^2 + (\Delta\phi_f)^2}. \quad (42)$$

The error $\Delta\phi_f$ is due to all the uncertainties in the data (38) over half the smoothing range (or less if the start of the numerics occurs within that range). The junction of the numerical region to the near-maximum series expansion generally occurs just where ϕ becomes unstable and $\Delta\phi$ starts to diverge, so it is essentially unnecessary to ever start adding the full $\Delta\phi$ errors directly instead of in quadrature.

It is assumed that the errors coming out of the origin series are zero, since in practice the actual errors are always miniscule compared with the estimated error beyond the first few points of the series. Beyond the maximum, in the second numerical integration region, the error due to the near-maximum series is not negligible, but this is slowly corrected by the natural stability of the ϕ DE, so that it decays from step to step as

$$\Delta\phi_s = \Delta\phi[i_0] - \sum_{j=i_0}^i \Delta\phi_z^*[j] \delta z, \quad (43)$$

where $\Delta\phi[i_0]$ is the error at the end of the near-maximum series, and $\Delta\phi_z^*$ is calculated from (22), reflecting how the error in ϕ acts to stabilize itself. Figure 3 contains a plot showing how the estimated error compares with the actual error in the propagation of the ϕ uncertainties.

The integrated r values come directly from the ϕ values, but the uncertainties have to take into account the uncertainties in all the ϕ values. Even when ϕ is stable and self-corrects when an error emerges, the integrated values of r all continue to be off by the amount gained or lost while the values of ϕ were in error. When ϕ fluctuates above and below the correct value, then the errors in the r values grow like a random walk. Thus, the error in r is calculated by adding all the previous errors due to ϕ in quadrature to account for how far it should have wandered due to the random high and low values of ϕ .

The integrated values of M are stable before the maximum in \hat{R} and then become unstable after the maximum due to the feedback with W . Thus, before the maximum, it is assumed that there is no M error in the calculation of the W error, and no W error in the calculation of the M error, so that these errors do not feed back on each other and depend solely on the $4\pi\mu n$, ϕ , \hat{R} , and \hat{R}_z errors. After the maximum, the W errors are included in the calculation of the M_z errors, and if the W values are being determined from the integrated values of M (rather than an extended series expansion for W), then the M errors need to be included in the calculation of the W errors as well.

V. DEALING WITH SYSTEMATIC ERRORS

It is very likely that there will be systematic errors in the observations as well as the evolution functions. We here investigate the effect of such errors, and show that the data functions $\hat{R}(z)$ and $4\pi\mu(z)n(z)$ must satisfy a consistency condition. We demonstrate how a discrepancy in this condition can be corrected in order to make the data and the numerical result self-consistent. However, it is not possible to determine from this process how much error is attributable to \hat{R} and how much to $4\pi\mu n$, or to discern whether the systematic errors vary with z .

A. Systematic error in the distance scale

We first consider a constant percentage error in \hat{R} only. In this case, the origin values of ϕ start correspondingly high or low, since ϕ goes as \hat{R}/z near the origin. Then by (21) the numerical integration of ϕ continues to be off since ϕ_z depends on a $\hat{R}_{zz}\phi/\hat{R}_z$ term. When the $4\pi\mu n\phi/(\hat{R}_z\hat{R})$ term in ϕ_z becomes significant, ϕ starts to correct itself since the errors in $1/(\hat{R}_z\hat{R})$ bias the integration of ϕ in the opposite sense, and the integration may even overcorrect if it proceeds long enough.

By (A3)-(A7) the erroneous \hat{R} values produce correspondingly high or low values in the near-maximum series for ϕ , but because of the correction that takes place before the maximum, there is generally a discrepancy between the numerical and series ϕ values so a close matching is not possible. This discrepancy is a clear indicator of an overall systematic error. Beyond the near-maximum series, the numerical integration is stable and starts to correct the value of ϕ , leading to a discontinuity in the slope of the ϕ curve, providing a secondary indication of a systematic error. Since the integrated values of r depend on the ϕ values, then if ϕ is too high (or low) over most of the run, then r tends to be correspondingly high (or low) over the whole run by approximately the percentage of the error in the \hat{R} values, but it is not obvious from the $r(z)$ curve that a systematic error is present.

The presence of a jump in ϕ at the start of the near-maximum series not only flags a systematic error, but also provides the means of correcting it. Thus, simply by systematically increasing or decreasing all of the \hat{R} values until the jump in ϕ is minimized, the best correction for \hat{R} can be found. The adjustment of the \hat{R} data necessitates a repeat of the entire integration from the origin to the maximum series matching point. The effects of a systematic error in \hat{R} on ϕ and r can be seen in Figure 4.

A systematic error in \hat{R} is also apparent in W . Initially, the values of W and M are unaffected by the \hat{R} values. The values of ϕ , \hat{R} , and \hat{R}_z are generally all correspondingly high or low, so when the $-M\phi/(\hat{R}\hat{R}_z)$ term in (25) starts to become significant, W becomes correspondingly too high or too low (and M in turn also becomes slightly too high or too low). However, when matching the numerical integration to the near-maximum series, the change in the value of $\hat{R}_m/2$ is greater than the percentage change in M , which influences the slope of the M series and the constant term of the W series such that M and W end up being correspondingly high or low in the ensuing numerical integration. Since the calculation of t_B depends on E and M , the jumps in W and M also typically lead to jumps in t_B . The effects of a systematic error in \hat{R} on W , M , and t_B can also be seen in Figure 4.

It should be noted however that only a constant correction can be made this way, and a z -dependent systematic error cannot be distinguished from a constant one. The ability to detect an accumulated systematic error and correct for it is due to the unique geometric properties of \hat{R}_m noted by Hellaby [29], and this locus is an exception to the theorem of Mustapha et al. [18].

If the systematic percentage error in \hat{R} grows with z , the effect at low z is qualitatively similar, but less pronounced near the origin. However, the maximum in \hat{R} is changed not only in magnitude \hat{R}_m , but also in redshift z_m . If this occurs, then the ϕ series is calculated opposingly low (or high) due to the higher (or lower) value of $4\pi\mu n$ at z_m . Then the subsequent numerical integration only asymptotically corrects the value of ϕ . Thus, the overall influence with ϕ being successively too high and too low for parts of the integration is that r may end up approximately correct at the end of the integration. Both M and W are not much changed before the series matching, but the shift in z_m opposingly decreases (or increases) the linear slope of the M series curve more than the high (or low) value in

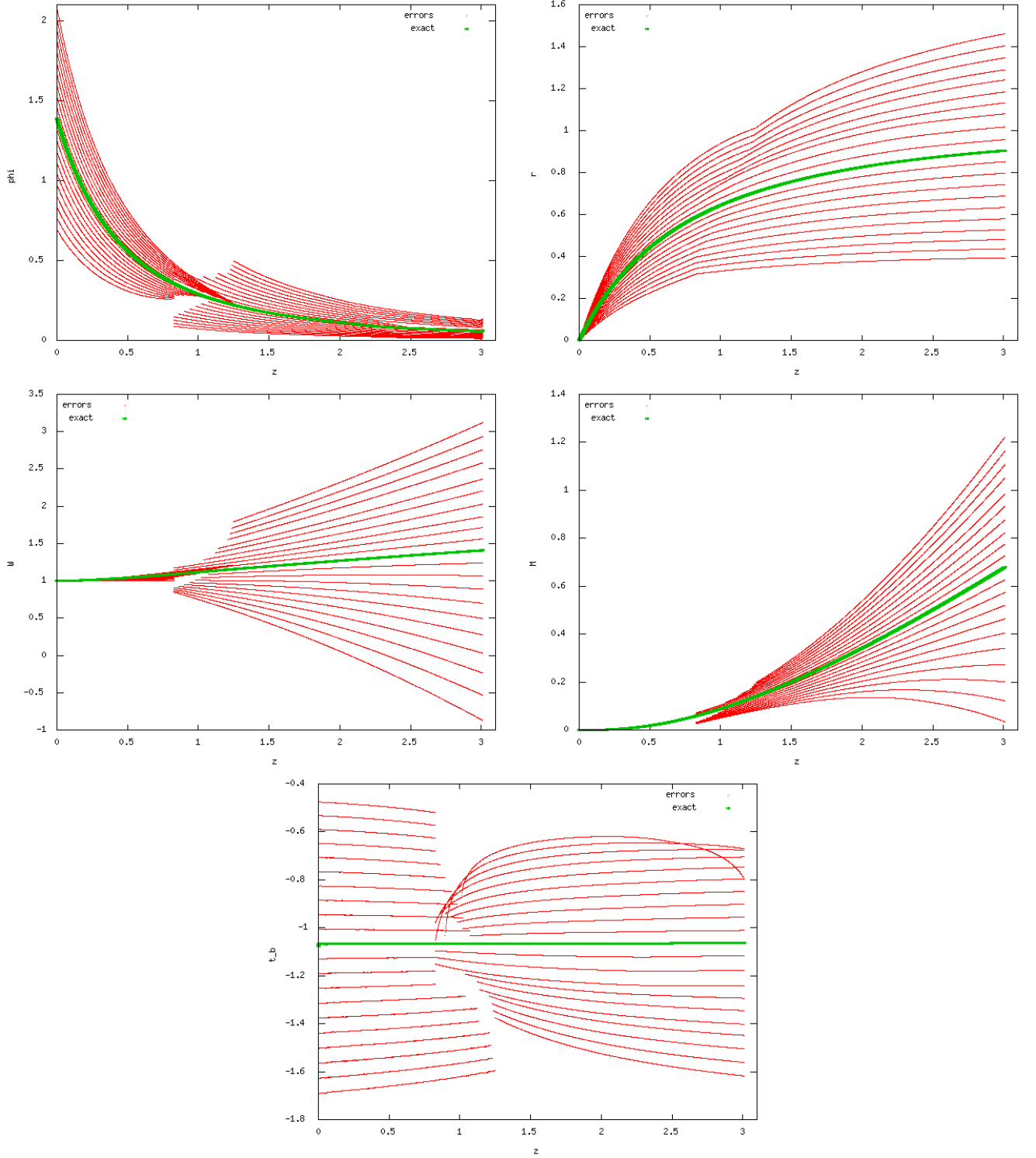


FIG. 4: Systematic errors in the data lead to an inconsistency when attempting to join numerical and near-maximum series regions, leading to jumps in ϕ , W , M and t_B . This is illustrated for a systematic error in \hat{R} only. The functions ϕ (top left), r (top right), W (middle left), M (middle right), and t_B (bottom) versus z are plotted with the exact data (thick line) and with various corrections of the systematic error (thin lines). Each subsequent curve represents a 5% difference in the correction of the \hat{R} data. The plots are for an FLRW universe with $h_0 = 0.72$, $q_0 = 0.22$, and $\Omega_\Lambda = 0$.

$M_m = \hat{R}_m/2$ decreases it. This makes the values of M and W too low (or high) when the numerical integration resumes after the near-maximum series expansion.

B. Systematic error in the redshift space density

With a fixed percentage error in μn , ϕ is initially unaffected, but eventually becomes correspondingly high (or low) when the $4\pi\mu n\phi/(\hat{R}\hat{R}_z)$ term in (21) becomes significant. The near-maximum series for ϕ is opposingly low (or high) at \hat{R}_m by (A3)-(A7). Coming out of the series, the subsequent numerical values of ϕ only asymptotically approach the correct value. Thus, with ϕ being both too high and too low in turns, the integrated values of r are not as far off by the end of the integration as with a systematic error in the distance scale. These effects can be seen in Figure 5.

The value of M is initially correspondingly high (or low), since it depends on the $4\pi\mu n$ values, but W correspondingly increases (or decreases) because of the $-M\phi/(\hat{R}\hat{R}_z)$ term. This causes M to be only marginally high (or low) at the matching, but enough that the linear slope of the M series (and constant term of the W series) is opposingly low (or high) so that this then continues throughout the final numerical integration. The effects on the W and M values also affects the t_B values. These effects can also be seen in Figure 5.

Again, the presence of a vertical jump in ϕ at the matching from numerical to near-maximum series regions is a distinctive feature of a systematic error in the data, which may be corrected by adjusting the μn data until the jump vanishes.

The results are largely the same for an error in μn that systematically grows with redshift, except that obviously the effects are smaller if there is no error to begin with and the effects only begin to manifest themselves at higher redshift.

C. Systematic errors in both distance and density

Realistically, we expect both \hat{R} and μn to suffer from systematic errors. The plots in Figure 6 show the effects when the \hat{R} values are all 10% too large and the $4\pi\mu n$ values are all 10% too small. If a correction is made to the \hat{R} values only, this leads to an overcorrection such that r and M are 10% too small and t_B is 10% too large, compared with the original model the data came from. If a correction is made to the $4\pi\mu n$ values only, this makes r and M 10% too large and t_B 10% too small. Once one correction has been made, there are no jumps left in the data, so it is not apparent any further correction needs to be made.

With identical constant percentage errors (say p) in both \hat{R} and $4\pi\mu n$, ϕ starts out correspondingly high or low, the ϕ series is only slightly off, and then the ϕ integration asymptotically approaches the correct value at the end. Thus, r is too low by nearly the same percentage error, p , over the whole run. The low $4\pi\mu n$ values tend to make M low, and the errors in the $-M\phi/(\hat{R}\hat{R}_z)$ term for W essentially cancel out so that W is correct. Since both the M matching value and the M series value at the maximum are correspondingly high or low, then the slope in the M series (and hence the intercept in the W series) is approximately correct, so M ends up being off by about p percent over the whole run. Thus, only in the special case where both the errors are systematically off by the same percentage in the same direction is the simple result obtained that r and M are both off by the same percentage. In that case, since there is no apparent jump in ϕ , there is no way of knowing that an error correction is necessary.

Therefore, in making corrections for systematic errors, it is only possible to ensure that the \hat{R} and μn data are consistent at the maximum, i.e. that the accumulated mass derived from the integration agrees with that deduced from \hat{R}_m .

VI. CONCLUSION

The idea of extracting metric information from cosmological observations has been investigated theoretically in many papers, but until now had never been turned into a practical procedure. Such a project began with Lu and Hellaby [28] in which the theoretical algorithm of Mustapha et al. [18] was turned into a numerical program that uses galaxy redshifts, luminosity or diameter distances, and density in redshift space, to determine the geometry of the Cosmos; that is, it extracts information about the spacetime metric. The program was tested with fake data for which the true spacetime metric was known, and successfully demonstrated the basic viability of the procedure. At this early stage of development, spherical symmetry is assumed in order to focus on issues such as the development of an appropriate numerical method. In developing this procedure, it became clear that there are four distinct integration

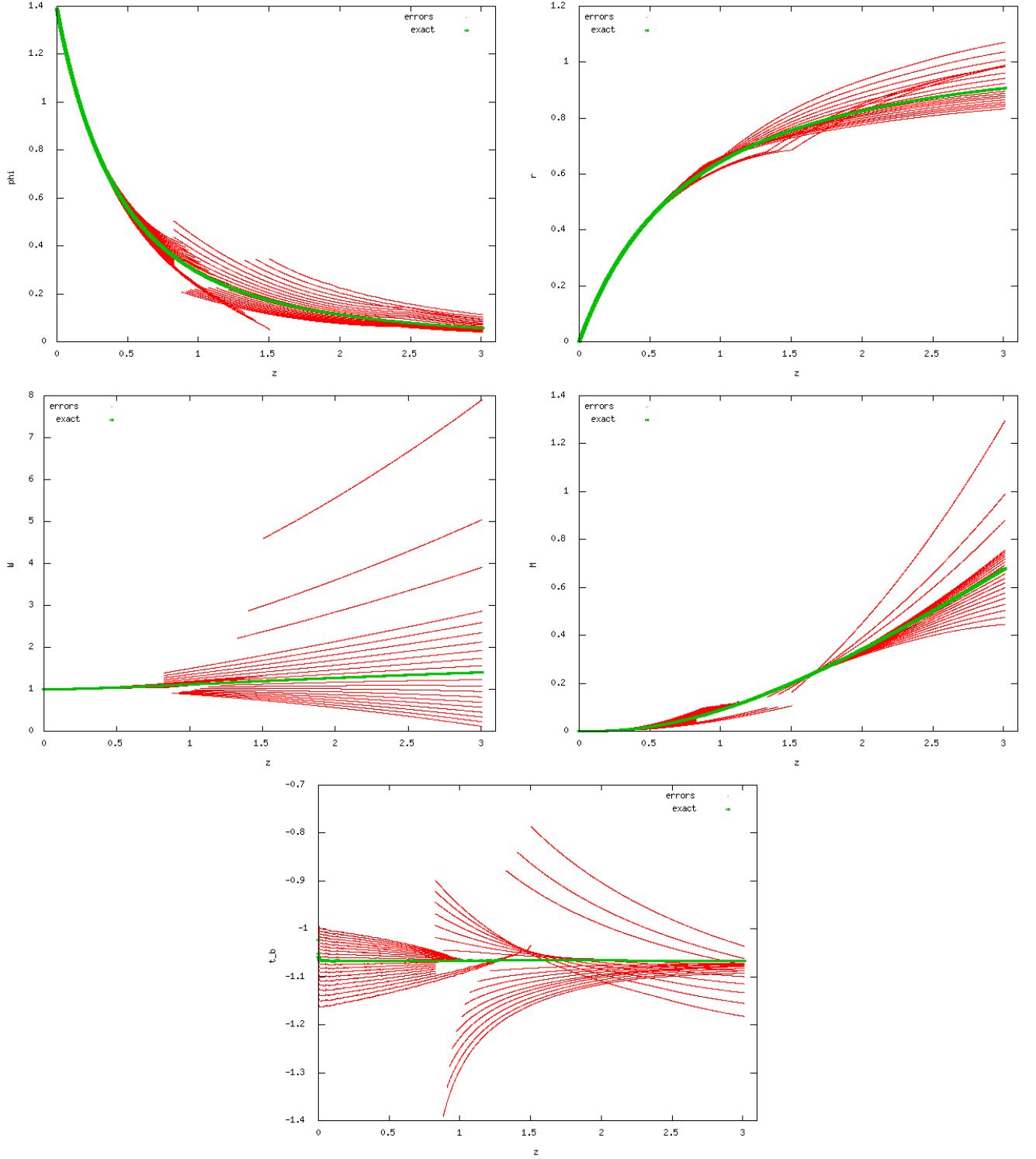


FIG. 5: Similar to Figure 4, but with a systematic error added to the $4\pi\mu n$ data instead of the \hat{R} data. The jumps due to various corrections of the systematic error in $4\pi\mu n$ are illustrated for the functions ϕ (top left), r (top right), W (middle left), M (middle right), and t_B (bottom) versus z , with the exact data (thick line) for comparison. Each subsequent curve (thin lines) represents a 5% difference in the correction of the $4\pi\mu n$ data. The plots are for an FLRW universe with $h_0 = 0.72$, $q_0 = 0.22$, and $\Omega_\Lambda = 0$.

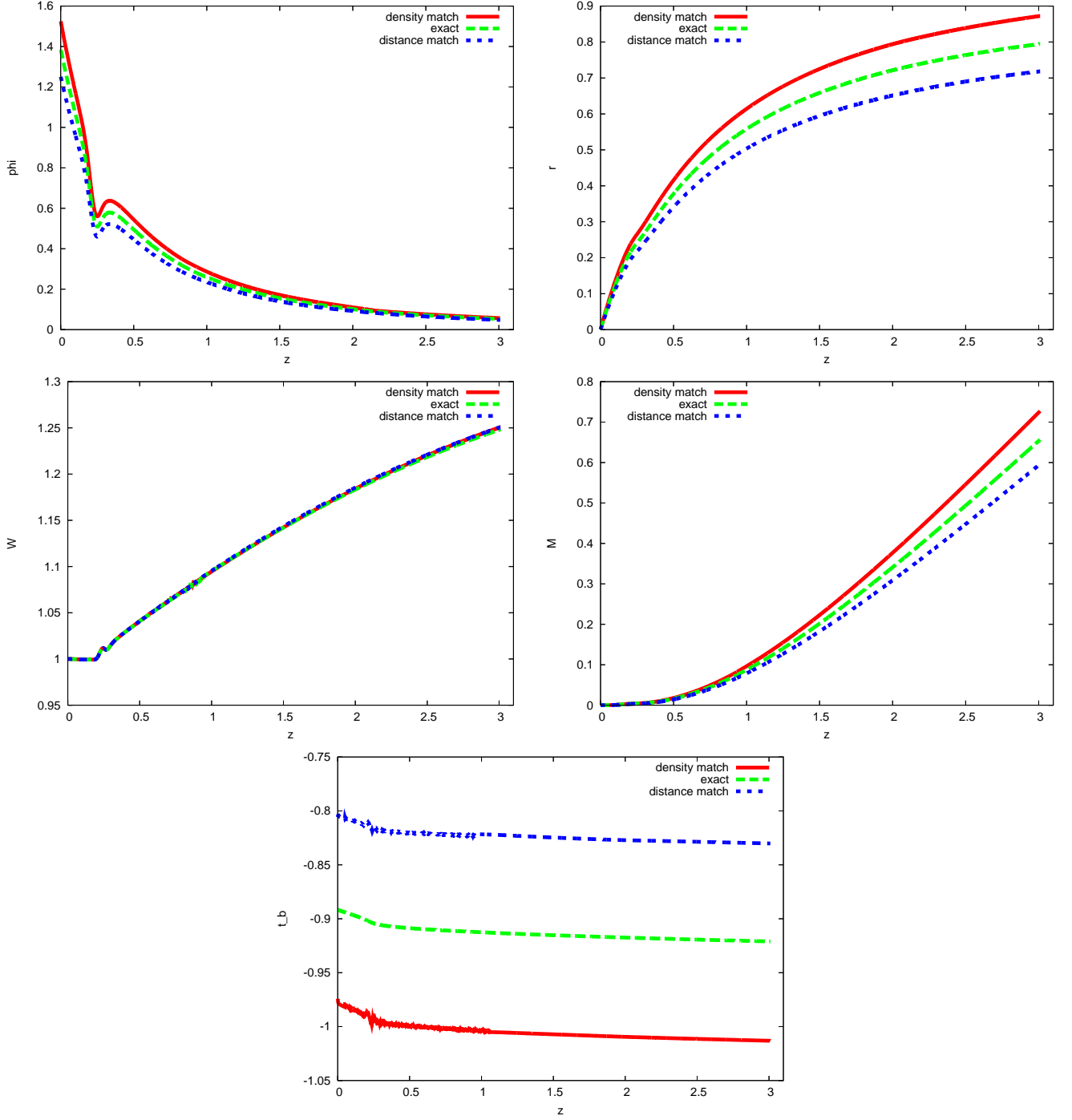


FIG. 6: Corrected curves with systematic errors added to both the \hat{R} and $4\pi\mu n$ data (+10% and -10% respectively). The plots show the exact data (dashes) and the corrected curves obtained by matching the curves for the \hat{R} data (dots) or $4\pi\mu n$ data (solid curve) to eliminate jumps. It is apparent the jumps may be removed by correcting either the \hat{R} or the $4\pi\mu n$ data. It is not possible to determine which correction should be made, but either result is much more self-consistent than with no correction. This is illustrated for the functions ϕ (top left), r (top right), W (middle left), M (middle right), and t_B (bottom) versus z . The plots of r , M , and t_B clearly end up overcorrected by 10% when a correction is made to one variable. These plots are for an inhomogeneous universe with origin parameters $h_0 = 0.72$, $q_0 = 0.6$, and $\Omega_\Lambda = 0$: a strong inhomogeneity is present around $z = 0.2 : 0.3$.

regions that require different treatment: setting up the initial values at the origin, a first numerical integration region, the neighbourhood of the maximum in the diameter distance, and a second numerical region.

The original code of Lu and Hellaby [28] has been modified to deal with statistical and systematic errors, and we have studied three consequences: how to estimate uncertainties in the metric functions, how data errors affect the stability of the integration process, and how a key consistency condition can be used to identify and partly correct for systematic errors. Simulated data were generated by adding Gaussian deviates to ideal data based on various homogeneous and inhomogeneous model universes, and this was used to test the new program. Significant improvements were needed in several aspects of the procedure. Because the DEs to be solved involve \hat{R}_{zz} , the second derivative of the data function \hat{R} , it is essential to smooth out observational noise by fitting a polynomial to \hat{R} over a range of z about each point. Without this, calculated R_{zz} values would suffer from gigantic errors. The estimation of the initial values at the origin was improved by using a small- z series expansion of the LTB metric, and fitting to a range of redshift bins near the origin. Also, the junctions between the numerical and near-maximum series expansion values for M and $W = \sqrt{1 + 2E}$ were improved so that numerical discrepancies were minimized.

An important result is the theoretical and numerical investigation of stability. The problem of integrating through the maximum in \hat{R} , where the DEs are singular, was already solved by Lu and Hellaby [28] by using a series expansion about \hat{R}_m . The numerical integration of $\phi(z)$ was here shown to be stable away from \hat{R}_m , and the region of serious numerical instability was avoided by the use of this series. The numerical integration of M and W , however, is only stable before \hat{R}_m is reached, and beyond this point errors in M and W feed back on each other. Because of this, it will be difficult to extend this integration far beyond \hat{R}_m unless another method can be found. We applied the quick fix of extending the near-maximum series for W to larger z values and combining it with the numerical integration of M , which removed the instability and gave acceptable results for the test models considered up to $z = 3$. However, such an approach must necessarily become increasingly inaccurate with z . We suspect however that this instability is not confined to the LTB model or spherical symmetry, but is a significant issue for analyzing high- z data, though the assumption of a homogeneous Robertson-Walker metric may hide the problem.

Particularly interesting was the effect of systematic errors. There is a relationship (18) (or its generalization (20)) between the mass and the diameter distance, that must hold at the maximum in \hat{R} . With data extending out past this maximum, it has been shown that it is possible to correct for an overall systematic error in either the distance ladder or the redshift matter density, making them mutually consistent at the maximum. Since a correction may be applied to either of the two data functions, $\hat{R}(z)$ and $\mu(z)n(z)$, there is a range of possible results. But the most likely systematic error will be in the redshift matter density, because the mass per source will be uncertain due to the fact that this mass has to include a component for all the material in the Universe that never collapsed to form objects, and for each source that we do see, there will probably be many smaller sources that we do not. Thus, it seems most logical to assume the distance ladder is correct and make the correction in the redshift matter density.

Our broad conclusion is that when sufficient cosmological data become available out towards a redshift $z \sim 2$, it should be possible to calculate the metric for the Cosmos, and thereby check homogeneity, at least within this range. With upcoming surveys, such data should be available in the not-too-distant future. At larger redshift values, well beyond \hat{R}_m at roughly $z \sim 1.5$, there is a difficulty with stability, potentially resulting in large errors, which we believe may be a general problem for analysis of high- z data, making it difficult to properly verify homogeneity on the largest scales. It is possible that another method might be devised to avoid this instability, but we have not found one.

Acknowledgments

We thank Byron Desnoyers Winmill for programming advice. MLM thanks South Africa's National Research Foundation for a postdoctoral fellowship. CH thanks the National Research Foundation for a research grant.

APPENDIX A: THE NEAR-MAXIMUM SERIES FOR THE PNC IN LTB MODELS

This appendix provides the solution for the LTB arbitrary functions as series in $\Delta z = z - z_m$ near $z = z_m$ where the maximum $R_m = \hat{R}(z_m)$ occurs. We write out all functions as power series in Δz :

$$\hat{R} = R_m + \sum_{i=2}^{\infty} R_i \Delta z^i, \quad 4\pi\mu n = K_m + \sum_{i=1}^{\infty} K_i \Delta z^i, \quad \hat{r} = r_m + \sum_{i=1}^{\infty} r_i \Delta z^i, \quad (\text{A1})$$

$$M = M_m + \sum_{i=1}^{\infty} M_i \Delta z^i, \quad \sqrt{1 + 2E} = W = W_m + \sum_{i=1}^{\infty} W_i \Delta z^i. \quad (\text{A2})$$

The coefficients in the \hat{R} and $4\pi\mu n$ series are found from polynomial fits to the data near the maximum in \hat{R} , and the coefficients of the series for \hat{r} , M , and W are obtained by substituting these series into the DEs (13), (17), (15), and (16). The following extends the results of Lu and Hellaby [28]. We find

$$\phi_0 = r_1 = \frac{-2R_m R_2}{K_m}, \quad (\text{A3})$$

$$\phi_1 = r_2 = \left(\left\{ \frac{K_1}{K_m} - \frac{1}{1+z_m} \right\} R_2 - 3R_3 \right) \frac{R_m}{K_m}, \quad (\text{A4})$$

$$\begin{aligned} \phi_2 = r_3 = & \left(\left\{ \frac{2K_2}{3K_m} - \frac{K_1^2}{2K_m^2} + \frac{2K_1}{3K_m(1+z_m)} + \frac{1}{2(1+z_m)^2} \right\} R_2 \right. \\ & \left. + \left\{ \frac{K_1}{K_m} - \frac{1}{(1+z_m)} \right\} \frac{3R_3}{2} - 4R_4 - \frac{2R_2^2}{3R_m} \right) \frac{R_m}{K_m}, \end{aligned} \quad (\text{A5})$$

$$\begin{aligned} \phi_3 = r_4 = & \left(\left\{ \frac{K_3}{2K_m} - \frac{2K_1 K_2}{3K_m^2} + \frac{K_1^3}{4K_m^3} + \frac{K_2}{2K_m(1+z_m)} \right. \right. \\ & - \frac{5K_1^2}{12K_m^2(1+z_m)} - \frac{K_1}{4K_m(1+z_m)^2} - \frac{1}{4(1+z_m)^3} \left. \right\} R_2 \\ & + \left\{ \frac{K_2}{K_m} - \frac{3K_1^2}{4K_m^2} + \frac{K_1}{K_m(1+z_m)} + \frac{3}{4(1+z_m)^2} \right\} R_3 \\ & + \left\{ \frac{K_1}{K_m} - \frac{1}{1+z_m} \right\} (2R_4) - 5R_5 \\ & \left. + \left\{ \frac{K_1}{6K_m} - \frac{1}{2(1+z_m)} \right\} \frac{R_2^2}{R_m} - \frac{3R_2 R_3}{2R_m} \right) \frac{R_m}{K_m}, \end{aligned} \quad (\text{A6})$$

$$\begin{aligned} \phi_4 = r_5 = & \left(\left\{ \frac{2K_4}{5K_m} - \frac{K_1 K_3}{2K_m^2} - \frac{2K_2^2}{9K_m^2} + \frac{K_2 K_1^2}{2K_m^3} - \frac{K_1^4}{8K_m^4} + \frac{2K_3}{5K_m(1+z_m)} \right. \right. \\ & - \frac{11K_1 K_2}{18K_m^2(1+z_m)} + \frac{K_1^3}{4K_m^3(1+z_m)} + \frac{K_1^2}{9K_m^2(1+z_m)^2} \\ & - \frac{K_2}{6K_m(1+z_m)^2} + \frac{K_1}{12K_m(1+z_m)^3} + \frac{1}{8(1+z_m)^4} \left. \right\} R_2 \\ & + \left\{ \frac{3K_3}{4K_m} - \frac{K_1 K_2}{K_m^2} + \frac{3K_1^3}{8K_m^3} + \frac{3K_2}{4K_m(1+z_m)} \right. \\ & - \frac{5K_1^2}{8K_m^2(1+z_m)} - \frac{3K_1}{8K_m(1+z_m)^2} - \frac{3}{8(1+z_m)^3} \left. \right\} R_3 \\ & + \left\{ \frac{4K_2}{3K_m} - \frac{K_1^2}{K_m^2} + \frac{4K_1}{3K_m(1+z_m)} + \frac{1}{(1+z_m)^2} \right\} R_4 \\ & + \left\{ \frac{K_1}{K_m} - \frac{1}{(1+z_m)} \right\} \frac{5R_5}{2} - 6R_6 \\ & + \left\{ \frac{2K_2}{45K_m} + \frac{19K_1}{90K_m(1+z_m)} + \frac{1}{6(1+z_m)^2} \right\} \frac{R_2^2}{R_m} \\ & + \left\{ \frac{7K_1}{20K_m} - \frac{23}{20(1+z_m)} \right\} \frac{R_2 R_3}{R_m} \\ & - \frac{3R_3^2}{4R_m} - \frac{26R_2 R_4}{15R_m} + \frac{8R_2^3}{45R_m^2} \left. \right) \frac{R_m}{K_m} \end{aligned} \quad (\text{A7})$$

$$M_m = \frac{R_m}{2} , \quad (\text{A8})$$

$$M_1 = M_1 , \quad (\text{A9})$$

$$M_2 = \left\{ \frac{K_1}{K_m} + \frac{1}{1+z_m} \right\} \frac{M_1}{2} - \frac{R_2}{2} - \frac{K_m^2}{2R_m} , \quad (\text{A10})$$

$$M_3 = \left\{ \frac{K_2}{K_m} + \frac{K_1}{K_m(1+z_m)} - \frac{R_2}{R_m} \right\} \frac{M_1}{3} - \left\{ \frac{K_1}{K_m} + \frac{1}{1+z_m} \right\} \frac{R_2}{4} - \frac{R_3}{4} - \frac{K_m K_1}{2R_m} , \quad (\text{A11})$$

$$M_4 = \left\{ \frac{K_3}{K_m} + \frac{K_2}{K_m(1+z_m)} - \frac{K_1 R_2}{K_m R_m} - \frac{R_3}{R_m} - \frac{1}{R_m(1+z_m)} \right\} \frac{M_1}{4} - \left\{ \frac{5K_1}{36K_m(1+z_m)} + \frac{2K_2}{9K_m} - \frac{K_1^2}{24K_m^2} - \frac{K_m^2}{6R_m^2} - \frac{1}{24(1+z_m)^2} \right\} R_2 + \frac{2R_2^2}{9R_m} - \left\{ \frac{K_1}{8K_m} + \frac{1}{8(1+z_m)} \right\} R_3 - \frac{R_4}{6} - \frac{K_1^2}{8R_m} - \frac{K_2 K_m}{3R_m} - \frac{K_m^2}{24R_m(1+z_m)^2} ; \quad (\text{A12})$$

and

$$W_m = \frac{M_1}{K_m} , \quad (\text{A13})$$

$$W_1 = \frac{M_1}{K_m(1+z_m)} - \frac{R_2}{K_m} - \frac{K_m}{R_m} , \quad (\text{A14})$$

$$W_2 = -\frac{R_2 M_1}{R_m K_m} + \left\{ \frac{K_1}{4K_m} - \frac{3}{4(1+z_m)} \right\} \frac{R_2}{K_m} - \frac{3R_3}{4K_m} - \frac{K_1}{2R_m} , \quad (\text{A15})$$

$$W_3 = -\left\{ R_3 + \frac{R_2}{(1+z_m)} \right\} \frac{M_1}{R_m K_m} + \left\{ \frac{K_2}{9K_m} - \frac{K_1^2}{12K_m^2} + \frac{2K_m^2}{3R_m^2} + \frac{7K_1}{36K_m(1+z_m)} + \frac{1}{6(1+z_m)^2} \right\} \frac{R_2}{K_m} + \frac{8R_2^2}{9R_m K_m} + \left\{ \frac{K_1}{4K_m} - \frac{1}{2(1+z_m)} \right\} \frac{R_3}{K_m} - \frac{2R_4}{3K_m} - \frac{K_2}{3R_m} - \frac{K_m}{6R_m(1+z_m)^2} . \quad (\text{A16})$$

- [1] G. Temple, Proc. R. Soc. London **A168**, 122 (1938).
- [2] W. H. McCrea, Z. Astrophys. **9**, 290 (1934).
- [3] W. H. McCrea, Z. Astrophys. **18**, 98 (1939) [Gen. Relativ. Gravit. **30**, 315 (1998)].
- [4] J. Kristian and R. K. Sachs, Astrophys. J. **143**, 379 (1966).
- [5] G. F. R. Ellis, S. D. Nel, R. Maartens, W. R. Stoeger, and A. P. Whitman, Phys. Reports. **124**, 315 (1985).
- [6] M. E. Araújo and W. R. Stoeger, Phys. Rev. D **60**, 104020 (1999) [erratum: Phys. Rev. D **64**, 049902 (2001)].
- [7] M. E. Araújo, R. C. Arcuri, M. L. Bedran, L. R. de Freitas, and W. R. Stoeger, Astrophys. J. **549**, 716 (2001).
- [8] M. E. Araújo, S. R. M. M. Roveda, and W. R. Stoeger, Astrophys. J. **560**, 7 (2001).

- [9] R. Maartens and D. R. Matravers, *Class. Quantum Grav.* **11**, 2693 (1994).
- [10] R. Maartens, N. P. Humphreys, D. R. Matravers, and W. R. Stoeger, *Class. Quantum Grav.* **13**, 253 (1996) [erratum: *Class. Quantum Grav.* **13**, 1689 (1996)].
- [11] W. R. Stoeger, S. D. Nel, R. Maarteens, and G. F. R. Ellis, *Class. Quantum Grav.* **9**, 493 (1992).
- [12] W. R. Stoeger, G. F. R. Ellis, and S. D. Nel, *Class. Quantum Grav.* **9**, 509 (1992).
- [13] W. R. Stoeger, S. D. Nel, and G. F. R. Ellis, *Class. Quantum Grav.* **9**, 1711 (1992).
- [14] W. R. Stoeger, S. D. Nel, and G. F. R. Ellis, *Class. Quantum Grav.* **9**, 1725 (1992).
- [15] N. Mustapha, B. A. C. C. Bassett, C. Hellaby, and G. F. R. Ellis, *Class. Quantum Grav.* **15**, 2363 (1998).
- [16] M. B. Ribeiro and W. R. Stoeger, *Astrophys. J.* **592**, 1 (2003).
- [17] V. V. Albani, A. S. Iribarrem, M. B. Ribeiro, and W. R. Stoeger, *Astrophys. J.* **657**, 760 (2007).
- [18] N. Mustapha, C. W. Hellaby, and G. F. R. Ellis, *Mon. Not. R. Astron. Soc.* **292**, 817 (1997).
- [19] G. Lemaître, *Ann. Soc. Sci. Bruxelles.* **A53**, 51 (1933) [*Gen. Relativ. Gravit.* **29**, 641 (1997)].
- [20] R. C. Tolman, *Proc. Nat. Acad. Sci. U.S.A.* **20**, 169 (1934) [*Gen. Relativ. Gravit.* **29**, 935 (1997)].
- [21] H. Bondi, *Mon. Not. R. Astron. Soc.* **107**, 410 (1947) [*Gen. Relativ. Gravit.* **11**, 1783 (1999)].
- [22] C. Hellaby, *Astron. Astrophys.* **372**, 357 (2001).
- [23] M.-N. Célérier, *Astron. Astrophys.* **353**, 63 (2000).
- [24] M.-N. Célérier, *New Adv. Phys.* **1**, 29 (2007).
- [25] M.-N. Célérier, [arXiv:0706.1029](https://arxiv.org/abs/0706.1029), to appear in Proceedings of the XIXth Rencontres de Blois, Matter and energy in the Universe, Blois, France, May 2007.
- [26] N. Bishop and P. Haines, *Quaestiones Mathematicae.* **19**, 259 (1996).
- [27] H.-C. Lu, M.Sc. Thesis, University of Cape Town, 2006.
- [28] T. H.-C. Lu and C. Hellaby, *Class. Quantum Grav.* **24**, 4107 (2007).
- [29] C. Hellaby, *Mon. Not. R. Astron. Soc.* **370**, 239 (2006).
- [30] G. F. R. Ellis, in *General Relativity and Cosmology: Proc. Int. School Phys. "Enrico Fermi" (Varenna) Course XLVII*, edited by R. K. Sachs (Academic Press, New York, 1971), p. 104.
- [31] I. M. H. Etherington, *Philos. Mag. VII* **15**, 761 (1933) [*Gen. Relativ. Gravit.* **39**, 1055 (2007)].
- [32] N. Mustapha and C. Hellaby, *Gen. Relativ. Gravit.* **33**, 455 (2001).
- [33] A. Krasinski and C. Hellaby, *Phys. Rev. D* **69**, 043502 (2004).
- [34] C. Hellaby, *Class. Quantum Grav.* **4**, 635 (1987).
- [35] W. H. Press, S. A. Teukolsky, W. T. Vetterling, and B. P. Flannery, *Numerical recipes in C++: the art of scientific computing*, 2nd ed. (Cambridge University Press, Cambridge, 2002), p. 294.